JB Journals.ASM.org

Physiological and Proteomic Analysis of *Escherichia coli* Iron-Limited Chemostat Growth

James Patrick Folsom,[a,b] Albert E. Parker,[b,c] Ross P. Carlson[a,b]

Department of Chemical and Biological Engineering,[a] Center for Biofilm Engineering,[b] and Department of Mathematical Sciences,[c] Montana State University, Bozeman, Montana, USA

Iron bioavailability is a major limiter of bacterial growth in mammalian host tissue and thus represents an important area of study. *Escherichia coli* K-12 metabolism was studied at four levels of iron limitation in chemostats using physiological and proteomic analyses. The data documented an *E. coli* acclimation gradient where progressively more severe iron scarcity resulted in a larger percentage of substrate carbon being directed into an overflow metabolism accompanied by a decrease in biomass yield on glucose. Acetate was the primary secreted organic by-product for moderate levels of iron limitation, but as stress increased, the metabolism shifted to secrete primarily lactate (~70% of catabolized glucose carbon). Proteomic analysis reinforced the physiological data and quantified relative increases in glycolysis enzyme abundance and decreases in tricarboxylic acid (TCA) cycle enzyme abundance with increasing iron limitation stress. The combined data indicated that *E. coli* responds to limiting iron by investing the scarce resource in essential enzymes, at the cost of catabolic efficiency (i.e., downregulating high-ATP-yielding pathways containing enzymes with large iron requirements, like the TCA cycle). Acclimation to iron-limited growth was contrasted experimentally with acclimation to glucose-limited growth to identify both general and nutrient-specific acclimation strategies. While the iron-limited cultures maximized biomass yields on iron and increased expression of iron acquisition strategies, the glucose-limited cultures maximized biomass yields on glucose and increased expression of carbon acquisition strategies. This study quantified ecologically competitive acclimations to nutrient limitations, yielding knowledge essential for understanding medically relevant bacterial responses to host and to developing intervention strategies.

Adaptation to nutrient limitation is a key driver of microbial fitness in medical, environmental, and industrial contexts (e.g., see references 1, 2, and 3). Nutrient-limited growth is fundamental to cellular biology, influencing (i) the elemental composition of microorganisms (4–7), (ii) the amino acid sequence of nutrient transporters (4, 8), and (iii) the amino acid sequence of highly expressed proteins (9). Iron-limited growth is of special interest in medical and marine sciences, where it is central to bacterial pathogenesis and global nutrient cycling, respectively. Iron is an essential nutrient for bacterial growth, with only rare documented exceptions (10, 11), and many naturally occurring environments have low iron bioavailability. First, under neutral aerobic conditions, the dominant form of iron in aqueous solutions is $Fe(OH)_3$, which has an extremely low solubility, 10^{-9} to 10^{-10} M (12–14). Secondly, in medical contexts, vertebrates use nutrient sequestration to defend against bacterial colonization in a strategy termed nutritional immunity (15–17); in fact, some pathogenic bacteria have evolved to interpret iron scarcity as an indicator of growth in a vertebrate host tissue and alter gene expression accordingly (18, 19).

Microorganisms have acquired strategies for acclimation to low iron bioavailability. The most basic mechanisms include (i) stockpiling iron when it is available in ferritin- or bacterioferritin-based iron reserve complexes for use when iron is scarce (20) and (ii) retrenchment, where physiological activities are reduced until the iron scarcity is relieved (21). Bacteria also utilize high-affinity siderophore-based iron capture methods, where low-molecular-mass (<1.5-kDa) iron-binding molecules, having iron binding constants on the order of 10^{20} to 10^{50} (22, 23), are secreted. When iron is bound to these siderophores, high-affinity membrane transporters (e.g., FepA, with an affinity constant for ferric enterobactin of <0.2 nM [24]) transport the iron into the microorganism's interior, where it is transferred to iron-trafficking proteins (25–27). Additionally, prolonged iron scarcity on evolutionary time scales can result in metabolic shifts toward enzymes that do not require iron; this has occurred in some marine bacteria that have adapted to the ocean's iron scarcity by using flavodoxin-based respiratory-chain enzymes instead of iron-containing ferredoxin-based enzymes (28).

Chemostat cultivation has aided the investigation of microbial responses to nutrient limitation (29). Chemostats are steady-state bioreactors where fresh medium addition is balanced exactly by removal of working medium. The design permits control of culture growth rates and establishment of reproducible growth conditions that can be limited by a single nutrient. Additionally, chemostat cultivation simplifies the analysis and quantification of physiological properties like biomass and metabolic by-product yields (e.g., see references 30 and 31) by avoiding some of the complexities of batch growth, such as time-dependent changes in biomass and metabolite concentrations, as well as changes in the type and severity of culturing stresses.

Two-dimensional electrophoresis (2-DE) is a powerful technique for separating complex protein mixtures (32) which is often combined with mass spectrometry and sequence database

Received 25 February 2014 **Accepted** 12 May 2014

Published ahead of print 16 May 2014

Address correspondence to Ross P. Carlson, rossc@erc.montana.edu.

Supplemental material for this article may be found at http://dx.doi.org/10.1128/JB.01606-14.

doi:10.1128/JB.01606-14

searches to identify proteins (33). The use of 2-DE-based proteomics to study *E. coli* is a mature field, with many studies detailing culturing condition-dependent protein abundance patterns (e.g., see references 34, 35, 36, 37, and 38). Combining the defined, reproducible steady-state chemostat culturing conditions with 2-DE proteomics is especially powerful for discovering microbial metabolic responses to stresses. For instance, this combination of methods has been used to study the *E. coli* response to carbon limitation (39), heat shock (36), and phage predation survival (40).

The study of nutrient limitation and its effects on microbial metabolism is an active area of research because of its central role in microbial proliferation, survival, and evolution, but many gaps in knowledge remain, even for the model organism *E. coli*. Batch growth studies of *E. coli* under iron-limited conditions are few and are limited to measuring non-steady-state physiological responses (20, 41, 42), while the two chemostat studies involving iron limitation did not examine acclimations to gradients of nutrient limitation (43, 44). *E. coli* proteomics studies of iron-limited conditions are also few and are focused solely on membrane protein fractions and from non-steady-state batch cultivation (43, 44). The present study is the first to quantify the physiological and proteomic responses of *E. coli* to a gradient of rigorously defined, steady-state, iron-limited chemostat growth conditions without the complicating aspects associated with chelation agents like EDTA.

The iron availability gradient tested growth conditions from modest to extreme iron limitation and was contrasted experimentally with a glucose-limited gradient. Microbial responses to nutrient limitation change in response to the type and degree of scarcity, as measured via shifts in metabolic by-products and protein abundance. This study reveals a physiological continuum of metabolic acclimations, providing fundamental insight into ecologically competitive responses to a range of growth-limiting nutrient stresses relevant to medical infections. The data are consistent with cellular economy theories that study microbial acclimation to nutrient limitation via the competitive investment of limiting resources like iron or carbon into essential metabolic pathways at the cost of catabolic efficiency (45–49).

MATERIALS AND METHODS

Strain and growth media. All experiments used wild-type *E. coli* K-12 substrain MG1655. Aliquots (1.8 ml) of *E. coli* MG1655 were stored at −80°C in 25% glycerol.

All experiments used M9 minimal medium with 2× standard phosphate concentrations for added buffering capacity (84.5 mM Na_2HPO_4, 44.1 mM KH_2PO_4, 8.6 mM NaCl, and 18.7 mM NH_4Cl) at pH 7.0 ± 0.05 (50). After the base M9 medium was autoclaved, 1 ml/liter of magnesium chloride solution (1 M $MgSO_4 \cdot 7H_2O$; final concentration, 1 mM), 10 ml $liter^{-1}$ of trace element stock [0.55 g $liter^{-1}$ $CaCl_2$, 0.1 g $liter^{-1}$ $MnCl_2 \cdot 4H_2O$, 0.17 g $liter^{-1}$ $ZnCl_2$, 0.043 g $liter^{-1}$ $CuCl_2 \cdot 2H_2O$, 0.06 g $liter^{-1}$ $CoCl_2 \cdot 6H_2O$, 0.06 g $liter^{-1}$ $Na_2MoO_4 \cdot 2H_2O$, 0.06 g $liter^{-1}$ $Fe(NH_4)_2(SO_4)_2 \cdot 6H_2O$, 0.2 g $liter^{-1}$ $FeCl_3 \cdot 6H_2O$; adjusted to a pH of <1 with HCl], and glucose were added. The iron-limited chemostat medium had a final glucose concentration of 0.028 mM (5 g $liter^{-1}$), while the glucose-limited chemostat medium had a final glucose concentration of 2.2 mM (0.4 g $liter^{-1}$).

Modifications in culture medium were required for iron-limited growth at chemostat dilution rates of 0.1 and 0.2 h^{-1}. High organic acid production necessitated reformulation of the medium to maintain a neutral pH at steady state. The phosphate salt concentrations were changed to 103.5 mM Na_2HPO_4 and 25.4 mM KH_2PO_4. This medium had a starting pH of 7.35 ± 0.05 and the total concentration of phosphate described above.

To create iron-limiting conditions, contaminating iron was removed from all items in contact with the culture and medium by immersion for >18 h in 2% hydrochloric acid, followed by a thorough rinsing with Nanopure water (17.8 MΩ/cm). Iron was omitted from the trace element mix and iron was removed from medium components using 125 g of Chelex 100 resin (Sigma, St. Louis, MO) packed into a 25-mm by 500-mm column (catalog no. K420401-2550; Fisher Scientific, Pittsburgh, PA). Medium components were pumped through the column at a flow rate of 4 cm min^{-1}. Concentrated glucose solutions (700 g/liter) were passed through the Chelex 100 column once, resulting in a final concentration of approximately 400 g/liter after a column rinse step (the exact concentrations were measured via HPLC). The magnesium chloride solution (1 M $MgSO_4 \cdot 7H_2O$) was passed once over 25 g of the magnesium form of the Chelex 100 resin. The trace element mix was not treated with the Chelex 100 column. The M9 base was mixed at 10× the working concentration, passed repeatedly through a freshly regenerated column of Chelex 100 until no further iron removal could be achieved (3 passages), and then diluted to 1× (~5-fold dilution because of Chelex column rinses). The resulting iron-limiting M9 medium contained iron at concentrations comparable to that in Nanopure water (17.8 MΩ/cm) (based on the iron assay described below). A 0.022 μM concentration of iron was added to the iron-limited M9 medium prior to use.

Determination of iron levels by inductively coupled plasma mass spectrometry (ICP-MS) was not effective due to phosphate interference; therefor, iron removal was monitored using a Ferene-based assay adapted from the work of Riemer et al. (51). Ferene was substituted for ferrozine to improve sensitivity. Briefly, the iron detection reagent consisted of 6.5 mM Ferene, 6.5 mM neocuproine hemihydrate, 2.5 M ammonium acetate, and 1 M ascorbic acid. The iron measuring protocol consisted of adding 100 μl of iron detection reagent to 1 ml of test solution; absorbance at 593 nm was determined after 30 min at room temperature. An identically treated Nanopure water sample was used for blanking (17.8 MΩ/cm). For glucose and magnesium solutions, iron was not detectable compared to the Nanopure blank. For the concentrated M9 base medium, A_{593} measurements of 0.00 ± 0.002 units were typical. Standard iron curves were constructed using the Fluka analytical iron standard for atomic absorption spectroscopy (AAS) (Sigma, St. Louis, MO). The detection limit of the assay was approximately 0.01 to 0.02 μM, meaning that the final M9 medium, after full dilution and before addition of iron salts, had a residual iron concentration ≤0.005 μM.

Chemostat operation. Nutrient stress severity was controlled using classic chemostat theory. Decreasing the chemostat dilution rate lowers the steady-state concentration of the growth-limiting substrate, increasing nutrient limitation stress (52, 53) (see the supplemental material for further discussion). Chemostats with 300 ml of medium were inoculated with 450 μl of *E. coli* K-12 MG1655 freezer stock and incubated without flow for at least 6 h of growth at 37°C until the reactors were turbid. The reactors were operated at four dilution rates (0.4, 0.3, 0.2, and 0.1 h^{-1}) under glucose- or iron-limiting conditions. Reactors were sparged with filter-sterilized air at 1 liter per minute and stirred at 250 rpm (LabDisc S1). Ambient air was humidified by preliminary sparging through sterile 37°C Nanopure water in order to prevent evaporation and the associated cooling in the reactors. A time course analysis of feed carboy medium iron concentrations revealed iron settled out of solution; continuous stirring of feed carboys alleviated this problem, as determined by the Ferene-based iron assay. Chelators, like EDTA, were not used to avoid confounding competition effects between cell receptors, siderophores, and chelating agents. The pH was monitored offline and maintained at 7.0 ± 0.2 during steady-state growth using the previously described 2× phosphate buffer concentrations. Chemostats were operated until cultures reached steady state, defined as at least three consecutive measurements of optical density at 600 nm (OD_{600}) (±~10% or less) for 2 to 3 residence times (residence time = 1/dilution rate). The different nutrient limitations and different

dilution rates took different numbers of residence times to achieve steady state based on this definition (6 to ~17 residence times). All experiments were kept to fewer than 20 total residence times to minimize the effect of genetic mutations on results. Each steady-state culture had at least 3 culturing samples collected over 2 to 3 residence times. Biomass samples for proteomics analysis were harvested from reactors at the conclusion of each experiment. At least three separate chemostats were grown to steady state and sampled for each combination of nutrient limitation and dilution rate.

Culture analysis. The coefficients 0.48 ± 0.02 and 0.50 ± 0.03 g cells (dry weight)/liter/OD_{600} unit were found to correlate cell dry weight to optical density for iron- and glucose-limited growth, respectively. Concentrations of glucose and cellular by-products (pyruvate, succinate, lactate, formate, and acetate) were determined using an Agilent 1200 series high-performance liquid chromatograph (HPLC) equipped with an Aminex HPX-87H column (Bio-Rad, Hercules, CA). The column was operated at 0.6 ml/min with a 0.005 M H_2SO_4 mobile phase, and the column temperature was set for each run to maximize the resolution of analytes (25 to 50°C). Glucose was detected with a refractive index detector, and organic acids were detected by a variable-wavelength detector set at 210 nm. Ammonium concentrations were measured using the Berthelot reaction (54, 55), adjusted to a microplate format. Levels of excreted enterobactin were analyzed using the chrome azurol S (CAS) assay, which measures competitive iron-binding capacity, a proxy for siderophores (56). DASGIP off-gas analysis of carbon dioxide and oxygen (Eppendorf, Hauppauge, NY) was attempted, but low cell densities and high chemostat sparge rates prevented meaningful measurements of changes in these variables.

Protein extraction. At the conclusion of the steady-state experiment, the reactors were placed on wet ice and the entire reactor contents were transferred to prechilled 50-ml conical tubes on wet ice. Cells were pelleted at 3,220 × *g* and 4°C for 30 min (Eppendorf 5810R; Eppendorf, Hauppauge, NY), washed three times in ice cold wash buffer (10 mM Tris, 5 mM magnesium acetate [pH 8.0]), and frozen at −80°C until lysis. The cells were resuspended in 1 ml of ice-cold lysis buffer (30 mM Tris, 140 mM NaCl) with added protease and phosphatase inhibitors (cOmplete Mini and PhosSTOP; Roche Applied Science, Indianapolis, IN), and sonicated on ice at a setting of 2.5, for 4 rounds of 15 1-s bursts, with 1 min rest on ice between rounds (Sonic model 100 dismembrator; Fisher Scientific, Pittsburgh, PA; ultrasonic converter with microtip; Misonix Inc., Farmingdale, NY). The suspensions were frozen and thawed after the 4th round, followed by a 5th round of sonication.

A membrane protein enriched fraction was prepared, by centrifugation (100,000 × *g* and 4°C in a Beckman Optima ultracentrifuge for 45 min), and the supernatant was used as the cytosolic fraction. The pellet was resuspended in 800 μl of 30 mM Tris (pH 8.5) and repelleted as before. This washed membrane pellet was resuspended in 1 ml of membrane rehydration buffer (30 mM Tris, 7 M urea, 2 M thiourea, 4% CHAPS, 1% ASB-14 [pH 8.5]). The protein in the cytosolic fractions was precipitated with 10 volumes of cold acetone (−20°C) and kept overnight in acetone at −80°C. The protein was pelleted at 3,220 × *g* and 4°C for 1 h, air dried, and resuspended in cytosolic rehydration buffer (30 mM Tris, 7 M urea, 2 M thiourea, 4% CHAPS [pH 8.5]). All protein fractions were quantified by a modified Bradford assay (Bio-Rad, Hercules, CA) using bovine IgG standards and stored at −80°C until labeling.

Multiplex 2-dimensional gels. Zdyes (JAV I 131 red fluorophore, JAV I 187 blue fluorophore, and BDR I 227 green fluorophore) (Zdye, LLC, Gallatin Gateway, MT) were used to differentially label proteins (57, 58) for 2-dimensional gel electrophoresis gels. Briefly, 100 μg of protein was diluted to 20 μl (5 μg/μl) with appropriate rehydration buffer and 2 μl of Zdye (0.4 nmol/μl in dry dimethylformamide) was added to each protein aliquot. Labeling was allowed for 30 min at room temperature in the dark and quenched with the addition of 1 μl of 10 mM lysine for 10 min. Three protein aliquots were combined, each with different Zdye fluorophores, and brought to 450 μl in rehydration buffer with 43 mM dithiothreitol and 0.5% IPG buffer. These combined labeled samples were loaded onto IPG strips (24 cm Immobiline DryStrips with a nonlinear pH range of 3 to 11; GE Healthcare).

IPG strips were passively rehydrated for 18 h in the dark at room temperature, loaded onto an IPGphor 3 isoelectric focusing (IEF) system (Ettan; GE Healthcare Life Sciences, Piscataway, NJ), and subjected to the IEF schedule described in Table S1 in the supplemental material. After IEF, the strips were frozen at −80°C until equilibration, reduction, and alkylation. Strips were reduced with 130 mM dithiothreitol (DTT) in 7 ml of equilibration buffer (1.5 M Tris [pH 8.8], 6 M urea, 30% [vol/vol] glycerol, and 4% SDS [wt/vol]) for 15 min. Following reduction, the strips were alkylated with 508 mM iodoacetamide for 15 min in 7 ml of equilibration buffer. Reduction and alkylation were performed at room temperature in the dark on an orbital shaker.

Gradient gels (1.5 mm thick) were cast in an Amersham 24-cm casting chamber, 9.5% to 16% acrylamide gels were used for the membrane fractions, and 9.5% to 18% gels were used for the cytosolic fractions. Strips were loaded onto gels and sealed with 0.5% agarose containing 1.4% (vol/vol) thioglycolate solution (10% [vol/vol] thioglycolate, 5% [vol/vol] β-mercaptoethanol, 21.2% [wt/vol] Tris) and bromophenol blue. Electrophoresis proceeded in the dark at 3 W per gel until the bromophenol blue dye front exited the gel. Gel images were acquired using a Typhoon Trio gel scanner (GE Healthcare Life Sciences, Piscataway, NJ) at a 200-μm resolution, using a photomultiplier tube (PMT) voltage sufficient to scan each Zdye in the gels at just below the threshold of pixel saturation. After scanning, the gels were fixed (10% [vol/vol] methanol, 7% [vol/vol] acetic acid) for 24 h and washed thoroughly with Nanopure water. Gels were sealed in polyethylene bags and stored at 4°C until spot picking.

Protein spot picking. Gels were stained with blue silver (59), and spots were cut by hand. The gel pieces were destained (25 mM NH_4HCO_3, 50% [vol/vol] acetonitrile) twice for 30 min with vortexing and dried completely in a SpeedVac, followed by rehydration with 20 μl Promega Trypsin Gold (12.5 ng/μl, in 25 mM NH_4HCO_3, 10% [vol/vol] acetonitrile [pH 8.0]) on ice for 30 min. After rehydration, excess liquid was removed, and the gel pieces were covered with 25 mM NH_4HCO_3, 10% (vol/vol) acetonitrile (freshly adjusted to pH 8.0) and incubated at 37°C overnight.

To recover the peptides, 100 μl of Nanopure water was added to the excised gel pieces after digestion and vortexed for 10 min, followed by 5 min in a sonication bath. This first extract was transferred to a new tube containing 10 μl of extraction solvent (50% [vol/vol] acetonitrile, 5% [vol/vol] formic acid). The gel pieces were then covered with fresh extraction solvent, vortexed, and sonicated as before. A third extraction was carried out in extraction buffer without sonication. The extracted samples were combined, reduced to a volume of about 20 μl by SpeedVac, and frozen at −80°C until analysis by mass spectrometry.

Mass spectrometry. An Agilent 6520 accurate-mass quadrupole-time of flight (Q-TOF) chip liquid chromatography-mass spectrometry (LC-MS) system (Agilent Technologies, Santa Clara, CA) was used to identify proteins. The chromatography was performed on an Agilent ProtID-Chip-150 II (G4240-62006) with a 150-mm-long separation column (Agilent Technologies, Santa Clara, CA). Ions were acquired in positive mode, with automatic tandem MS (MS/MS). Solvents were water and acetonitrile, each containing 0.1% formic acid, and the organic fraction was increased linearly from 5% to 75% over 18 min and held at 75% for 9 min.

Mass spectrometry results were exported in mzData format and submitted to the MASCOT web server maintained by Matrix Sciences. The Swiss-Prot and NCBI nonredundant (nr) databases were searched based on theoretical tryptic digests with up to 3 missed cleavages, and taxonomy was restricted to *E. coli*. The variable protein modifications accounted for were carbamidomethylation of cysteine, asparagine and glutamine (NQ) deamidation, and oxidation of methionine. Peptide and MS/MS tolerances were set initially at ±50 ppm and ±0.2 Da, respectively, and tightened if necessary to achieve a <0.005% false detection rate (FDR) from

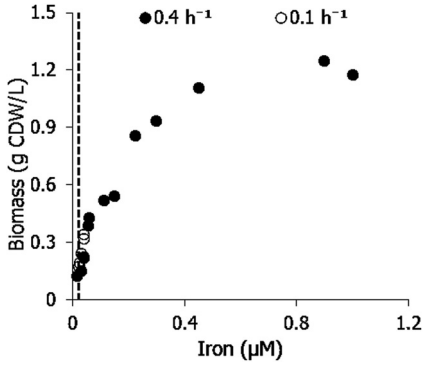

FIG 1 Steady-state chemostat *E. coli* cell density (g of cells [dry weight]/liter) as a function of iron added to glucose M9 minimal salts medium. Each circle represents a single biological replicate, i.e., a distinct chemostat experiment. The dashed vertical line (at 0.022 μM) represents the concentration of iron in the basal medium used for all subsequent iron-limited experiments. Chemostat dilution rate and specific growth rate are equivalent at steady state. CDW, cell dry weight.

the automatically generated inverse decoy database. Peptide matches were monoisotopic and allowed for charges of +1, +2, and +3. Proteins were considered identified if the FDR was <0.005% and there was at least one peptide with an expect score of <0.05. The supplemental material contains the results from MASCOT for the identified protein spots.

Protein abundance statistics. Chemostat cultures were operated under iron and glucose limitation at four different dilution rates (0.1, 0.2, 0.3, and 0.4 h^{-1}). Each of these eight distinct conditions was run in triplicate. Cytoplasm- and membrane-enriched protein from each independent triplicate was extracted. Three aliquots were taken from each of these 48 protein samples (eight conditions, triplicate experiments, and two protein fractions), and each aliquot was labeled with one of the three Zdye labels. Protein from iron-, glucose- and ammonium-limited samples grown at the same dilution rate and stained with compatible Zdye labels were separated on the same gel (ammonium limitation is not discussed here). The gels were scanned three times, once for each specific Zdye label. Typhoon imaging of the gels resulted in grayscale TIFF images of spots labeled with each Zdye label. The number of gel images for each of the 8 culturing conditions is indicated in the supplemental material; some conditions included more images. Images were loaded into Progenesis Samespots (v. 3.0.2966.28996) as a single-color experiment for alignment of gels and statistical analysis of the spot volumes. After alignment, only spots that yielded distinct mass spectrometry identifications and alignments were analyzed by Progenesis statistics ($n = 211$). Relevant groupings and pairwise-comparison groups were designed, and Progenesis statistics were run on these groups. This process was performed separately for the cytoplasmic and membrane protein fractions. All spot volume data from Progenesis and complete Progenesis statistics can be found in the supplemental material.

RESULTS

Establishing iron-limited chemostat growth. A series of chemostat experiments with successively lower medium iron concentrations was performed to validate iron-limited growth conditions. Extensive purification of the media and reactor components was required to establish iron-limited conditions. Figure 1 shows the steady-state chemostat cell density (g cell [dry weight]/liter) as a function of medium iron concentration. At iron concentrations below 0.5 μM, the cultures demonstrated iron-limited growth, as illustrated by the decreasing steady-state cell concentration. For these conditions, the chemostat effluent iron concentration was below the detection limits of the Ferene-based method (51).

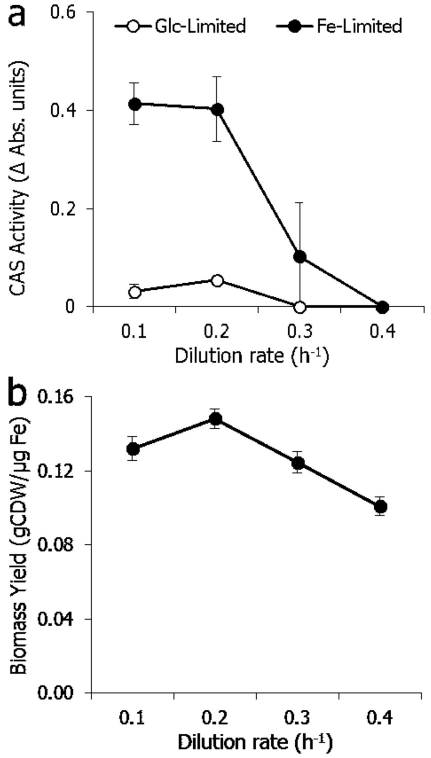

FIG 2 (a) Steady-state siderophore effluent concentrations based on the CAS competitive iron binding capacity assay as a function of chemostat dilution rate and limiting nutrient. Error bars show standard errors of the mean (SEM; $n = 4$, except $n = 3$ for 0.1 h^{-1} Fe-limited cultures). (b) Biomass per iron yield for the iron-limited cultures as a function of chemostat dilution rate. Data are means and SEM for three biological replicates. CDW, cell dry weight.

Analysis of iron-limited growth. A medium iron concentration of 0.022 μM, which resulted in a steady-state cell density equivalent to an OD_{600} of ~0.3 to 0.4, was used for all further reported studies. Iron-limited cultures at four dilution rates (D; 0.4, 0.3, 0.2, and 0.1 h^{-1}) were compared to glucose-limited cultures at the same dilution rates. Glucose-limited reactors were constrained to the same OD_{600} range using 0.4 g/liter glucose instead of the 5 g/liter glucose used for iron-limited experiments. Low cell densities were selected to prevent oxygen transfer limitation during chemostat experiments.

Iron-limited chemostat effluent was analyzed for glucose and ammonium; residual concentrations verified the cultures were not limiting for the nutrients. Analysis of glucose-limited reactor effluents for iron and ammonium verified that the cultures were not limiting for the nutrients.

Siderophore analysis and biomass yield on iron. The relative concentration of siderophore was measured using the chrome azurol S (CAS) competitive iron-binding capacity assay (56) (Fig. 2a). *E. coli* K-12 produces only one siderophore, enterobactin; therefore, assay results were assumed to be a result of secreted enterobactin (60). Values in Fig. 2a are plotted with respect to the difference in absorbance measurements between medium and effluent and reflect qualitative trends in siderophore concentrations. Iron-limited cultures had higher steady-state siderophore concentrations than glucose-limited cultures. The magnitude of siderophore concentration increased with decreasing dilution rate until 0.2 h^{-1}. A decrease in dilution rate translated into a lower

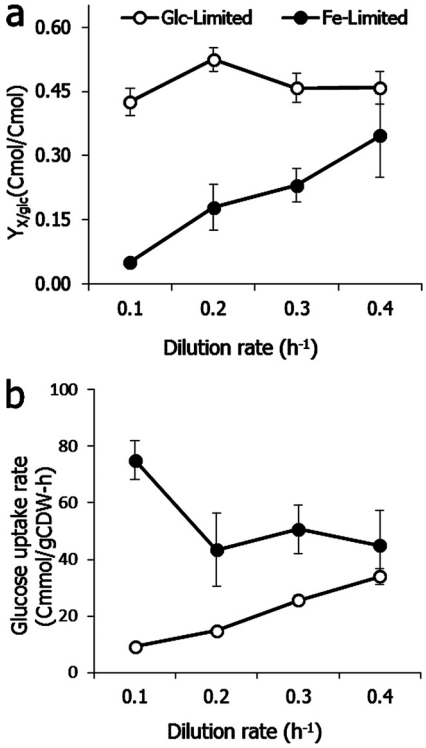

FIG 3 (a) Biomass yield on glucose ($Y_{X/glc}$) as a function of chemostat dilution rate and limiting nutrient. Data are means and SEM; $n \geq 4$. Biomass carbon composition was obtained from experimental CHNO elemental analysis. (b) Steady-state specific glucose uptake rate as a function of chemostat dilution rate and limiting nutrient. Data are means and SEM; $n \geq 4$. CDW, cell dry weight.

steady-state iron concentration and therefore increased nutrient limitation stress; steady-state siderophore concentrations were a balance between synthesis and loss in the effluent (the relevant theory is presented in the supplemental material). Consistent with previous research, glucose-limited cultures had a higher-than-background siderophore concentration for the lower dilution rates (61).

Biomass yield on iron was calculated for the iron-limited cultures (Fig. 2b). The data show a trend toward more efficient use of iron (as defined by g cells produced per μg iron assimilated) with increasing iron scarcity. When the iron limitation stress increased from a dilution rate of 0.4 to 0.2 h^{-1}, the biomass yield on iron increased (i.e., less iron per g of cells). The trend then declined slightly between dilution rates of 0.2 and 0.1 h^{-1}. The biomass iron content is approximately one-half the levels reported previously for iron-limited batch *E. coli* growth (20). Contaminating iron found in medium components, cell pellet rinse solutions, and reactor equipment prevented similar yield calculations from being performed for the glucose-limited cultures.

Biomass yields on glucose and specific glucose uptake rates. Two important physiological parameters associated with glucose metabolism, biomass yield on glucose and specific glucose uptake rate, are plotted in Fig. 3. Culture biomass yields on glucose (Cmole biomass/Cmole glucose, where Cmole is carbon moles) were a function of dilution rate and nutrient limitation (Fig. 3a). Biomass per glucose yields for the iron-limited cultures decreased with decreasing dilution rate (i.e., more severe nutrient limitation stress). The iron-limited conditions created higher levels of apparent nutrient stress than the glucose-limited condition at the same dilution rate. The iron-limited culture biomass per glucose yield was also more sensitive to decreases in dilution rate, as represented by the larger slope; relatively small changes in dilution rate resulted in large changes in stress. Under glucose limitation, *E. coli* converted the scarce resource glucose into biomass more efficiently than with iron-limited growth at each dilution rate (Fig. 3a).

Figure 3b plots culture-specific glucose consumption rates as a function of nutrient limitation and chemostat dilution rate. Specific glucose uptake rates increased in the iron-limited cultures with decreasing dilution rate (equivalent to specific growth rate). This is in contrast to the glucose-limited conditions, where the specific glucose consumption rate decreased with decreasing dilution rate. Biomass per glucose yield and specific glucose uptake rate are related via the culture growth rate (the theory can be found in the supplemental material).

Metabolic by-product profiles. *E. coli* has a flexible central metabolism, capable of a wide variety of fluxes which balance cellular mass, energy, and electron pools as a function of nutrient stress (39, 45, 46). Profiles of by-product yield per glucose changed significantly with both dilution rate and nutrient limitation (Fig. 4). Figure 4 plots the fraction of metabolized glucose carbon that was partitioned to acetate, lactate, pyruvate, and formate. Succinate was measured, but concentrations were low and are not included in Fig. 4 (data can be found in the supplemental material). Neither ethanol nor citrate was observed during HPLC analysis of culture effluent. The decrease in biomass per glucose yield (Fig. 3a) corresponded to an increase in organic by-product secretion, predominantly lactate. Iron-limited cultures grown at a dilution rate of 0.4 h^{-1} secreted primarily acetate (~25% of consumed glucose carbon) (Fig. 4a). With decreasing dilution rate, the by-product profile shifted; the fraction of glucose carbon secreted as acetate decreased, while the fraction of glucose carbon secreted as lactate and pyruvate increased (Fig. 4b and c). At a dilution rate of 0.1 h^{-1}, approximately 70% of the glucose carbon was secreted as lactate. Iron-limited growth (as well as severely glucose-limited growth) also produced measurable formate (Fig. 4d). While often associated with anaerobic growth, the secretion of formate under aerobic conditions has been reported previously (62, 63). The measured biomass and by-products accounted for ~80% of the iron-limited cultures' carbon and electrons at D of 0.1 h^{-1} (see Table S2 in the supplemental material).

Glucose-limited cultures, with their higher biomass-per-glucose yields, did not produce appreciable amounts of reduced carbon by-products (except for formate at a D of 0.1 h^{-1}). The glucose was either fully oxidized to carbon dioxide or incorporated into biomass. Published studies have reported that oxygen-limited *E. coli* cultures secrete reduced carbon by-products, like acetate (64, 65). The data presented here show no acetate production under glucose limitation, suggesting that oxygen was not limiting under any of the examined glucose-limited growth conditions. Specific oxygen consumption rates were calculated for all culture conditions using electron balances (see Table S2 in the supplemental material). The calculated specific oxygen consumption rate at a D of 0.1 h^{-1} for the glucose-limited culture was ~4-fold lower than that at a D of 0.4 h^{-1}; the observed formate secretion at a D of 0.1 h^{-1} was the result of a metabolic acclimation to limiting glucose, not oxygen limitation. Interesting, while the oxygen per

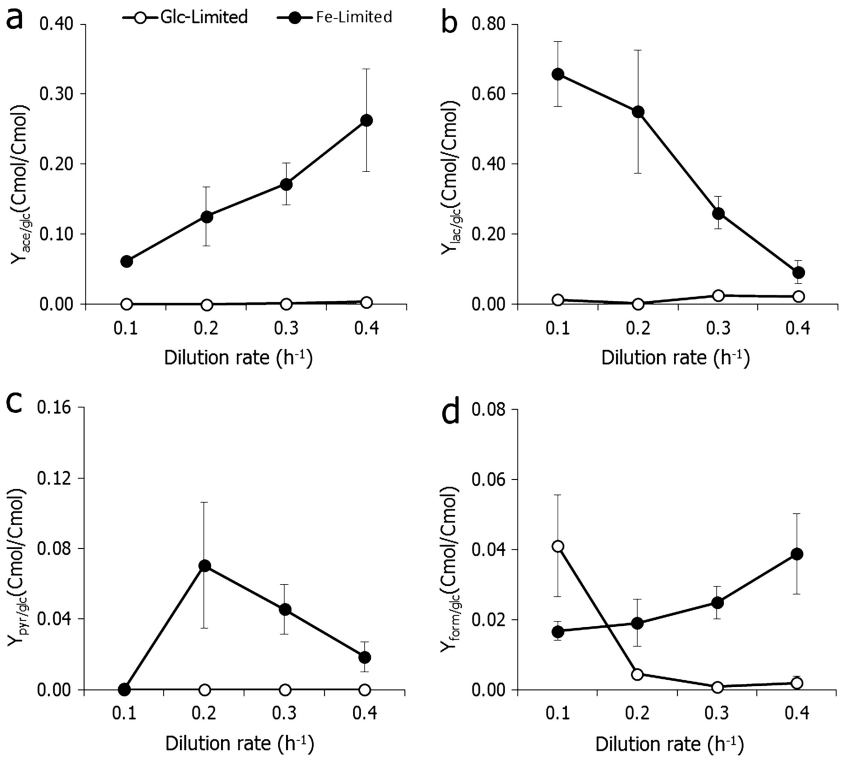

FIG 4 Culture by-product carbon yields (a) acetate, (b) lactate, (c) pyruvate, and (d) formate as a function of dilution rate and culture conditions. Data are means and SEM; $n \geq 4$.

Cmole of glucose yields for the iron-limited cultures were approximately half that of the glucose-limited cultures, the calculated specific oxygen consumption rates for the iron-limited cultures, with their high by-product yields, were as high as those in the carbon-limited cultures (see Table S2 in the supplemental material). This was the result of the increasing specific glucose uptake rate with decreasing dilution rate (Fig. 3b); similar behavior was observed previously for ammonia-limited *E. coli* growth (66). Additional presentations of the physiological data can be found in Table S2 in the supplemental material.

Proteomic analysis. Proteomic analysis of chemostat cell pellets was performed in conjunction with the physiological analysis. Cell pellets were fractionated into cytoplasmic and membrane samples, labeled with Zdye, and separated using differential 2-dimensional gel electrophoresis. Figure S1 in the supplemental material shows representative cytosolic and membrane protein gels, respectively, from iron- and glucose-limited chemostat cultures. A number of the identified protein spots are labeled for orientation and mapping purposes.

A total of 624 protein spots were distinguished in the membrane fractions and 896 protein spots in the cytoplasmic fractions based on Typhoon Trio image analysis of Zdye-labeled proteins. Table 1 lists the number of protein spots (including unidentified spots) that had more than a 2-fold spot intensity change across the conditions tested. Protein abundance differences between iron- and glucose-limited conditions were greatest at the lower dilution rates.

All protein spots visible on blue silver-stained 2-dimensional gels were manually excised and analyzed via mass spectrometry (MS) for identification. Manual visual analysis of blue silver-stained gels was less sensitive than the Typhoon Trio-based imaging of the Zdye-labeled gels. One hundred protein spots from the membrane fractions and 111 protein spots from the cytoplasmic fractions were identified via MS. Twenty-two spots from the membrane fractions and 24 spots from the cytoplasmic fractions contained MS peptide signatures from more than one protein. Considering identified proteins from both fractions (211 total proteins), 81.9% of the proteins demonstrated an abundance change of 2-fold or more for at least one of the pairwise comparisons (80% membrane, 83% cytoplasmic).

Numerous proteins were found in more than one location on

TABLE 1 Two-way comparisons for the total number of protein spots with >2-fold changes in abundance, considering all detected spots for iron (Fe)- and glucose (Glc)-limited chemostat growth

Comparison	No. of spots in:			
	Membrane fraction		Cytoplasmic fraction	
	Increase	Decrease	Increase	Decrease
Fe 0.1 h^{-1} vs Glc 0.1 h^{-1}	62	105	85	113
Fe 0.2 h^{-1} vs Glc 0.2 h^{-1}	88	82	84	93
Fe 0.3 h^{-1} vs Glc 0.3 h^{-1}	46	63	32	66
Fe 0.4 h^{-1} vs Glc 0.4 h^{-1}	63	64	33	64
Fe 0.1 h^{-1} vs Fe 0.4 h^{-1}	51	48	60	77
Fe 0.2 h^{-1} vs Fe 0.4 h^{-1}	51	69	63	87
Fe 0.3 h^{-1} vs Fe 0.4 h^{-1}	14	24	26	30
Glc 0.1 h^{-1} vs Glc 0.4 h^{-1}	87	55	81	87
Glc 0.2 h^{-1} vs Glc 0.4 h^{-1}	57	83	75	101
Glc 0.3 h^{-1} vs Glc 0.4 h^{-1}	27	16	30	23

the gels and were believed to represent protein isoforms with different posttranslational modifications likely used to modulate enzyme activity as a function of environmental cues (see Tables S3 and S4 in the supplemental material). For the cytosol fractions, 30 of 71 identified proteins had isoforms in more than one spot, while 27 of 107 proteins from the membrane fractions were found in more than one spot. The supplemental material provides an explicit accounting of all measured protein isoforms, MASCOT protein identification data, dilution rate- and nutrient limitation-based abundance profiles with results of statistical analysis, and a heat map of all identified proteins with hierarchical clustering.

Central metabolism protein abundance during iron-limited growth. Isoforms of key enzymes in the glycolytic pathway were upregulated under iron-limiting conditions, including at least one isoform of glyceraldehyde 3-phosphate dehydrogenase (GapA), phosphoglycerate kinase (Pgk), enolase (Eno), and pyruvate kinase (PykF), as well as the formate-producing pyruvate formate lyase (PflB) (Tables 2 and 3). For instance, the membrane isoform of GapA (ID 0261) was 2- to 3-fold higher ($P < 1.1 \times 10^{-16}$) during iron-limited growth at all dilution rates than under glucose-limited conditions. Protein levels for the cytoplasmic isoform of GapA (eID 1343) increased with decreasing dilution rate during iron-limited growth; protein levels were 3-fold higher ($P < 1.1 \times 10^{-16}$) at a D of 0.1 h^{-1} than 0.4 h^{-1} and were 2-fold higher ($P < 0.03$) under iron limitation at a D of 0.1 and 0.2 h^{-1} than those during glucose-limited growth. Pgk (eID 0666), found in the membrane fractions, was expressed at 2- to 4-fold higher levels ($P < 0.01$) under iron limitation than glucose limitation for all dilution rates. Two isoforms of Eno were found in the membrane (eID 1247 and ID 0145); levels of eID 1247 were 1.8- to 5.7-fold greater under iron limitation ($P < 1.1 \times 10^{-16}$). PykF (eID 0967) was found in the cytoplasmic fraction and was upregulated 2.5-fold under iron limitation at 0.1 h^{-1} ($P < 1.1 \times 10^{-16}$). PflB (ID 0200) was expressed at higher levels during iron limitation at all dilution rates except 0.1 h^{-1}. These observed trends were for selected isoforms; each protein had additional isoforms. Complete isoform data and results of statistical analyses can be found in Tables S3 and S4 in the supplemental material.

Abundance of key tricarboxylic acid cycle (TCA) enzymes contrasted sharply with abundance of glycolytic enzymes under iron-limited growth. Citrate synthase (GltA; eID 2245) abundance was down 3-fold ($P < 1.1 \times 10^{-16}$) at all dilution rates under iron-limited growth compared to glucose-limited growth. The membrane and cytosolic succinyl-CoA synthetase (SucD; eID 0852 and 0568) had protein abundance levels that were down 4- to 5-fold during iron limitation ($P < 1.1 \times 10^{-16}$) at all dilution rates. The data were indicative of reduced flux through the TCA cycle under iron-limited conditions. The abundance of aconitase B (AcnB) increased sharply at lower dilution rates for both iron- and glucose-limited cultures. The AcnB abundance increased 2.2-fold from a D of 0.4 h^{-1} to 0.1 h^{-1} for iron-limited growth ($P < 1.1 \times 10^{-16}$) and increased 2-fold from a D of 0.3 h^{-1} to 0.1 h^{-1} for the glucose-limited cultures ($P < 0.02$). The iron-limited cultures had higher AcnB abundance than the glucose-limited cultures at a D of 0.2 h^{-1} and 0.1 h^{-1}, while there was no statistically significant difference at the other dilution rates.

A few enzymes from the electron transport chain were identified from the 2-dimensional gels (see the supplemental material). Alternative quinone oxidoreductase (Qor; eID 0592) was expressed at 2-fold-higher levels ($P < 0.01$) under iron limitation at all dilution rates except 0.2 h^{-1}. The quinone oxidoreductase (WrbA) membrane isoform (eID 0824) was expressed at levels 2-fold lower ($P < 1.1 \times 10^{-16}$) than under glucose-limited conditions at dilution rates of 0.3 to 0.4 h^{-1}. The WrbA cytoplasmic isoform (eID 0443) did not show significant differences between nutrient limitations except at D of 0.1 h^{-1}.

Many enzymes associated with oxidative stress and oxygen radicals were also generally downregulated under iron limitation compared to glucose-limited growth, including superoxide dismutases (Sod). SodA (eID 1676) protein levels decreased 2-fold ($P < 1.1 \times 10^{-16}$) under iron-limiting conditions at a D of 0.1 h^{-1} compared to the glucose-limited culture, and SodB (eID 0099) protein abundance was 3-fold lower ($P < 1.1 \times 10^{-16}$) under iron-limiting conditions at all dilution rates except 0.4 h^{-1} than during glucose-limited growth. The DNA-binding protein Dps isoforms (ID 0571 and eID 2195), which have a role in anti-oxidative stress, had protein abundance levels 2- to 5-fold lower ($P < 1.1 \times 10^{-16}$) under iron-limited conditions than glucose-limited conditions at a D of 0.1 h^{-1}. Glutamate decarboxylase (GadAB) was found in the membrane and the cytoplasmic fractions. The membrane isoform of GadAB (eID 0742) had protein levels 2- to 3-fold higher during iron-limited growth from a D of 0.2 to 0.4 h^{-1}. The cytoplasmic isoform (eID 0915) had significantly higher protein levels only at a D of 0.2 h^{-1} (2-fold; $P < 1.1 \times 10^{-16}$). GadAB diverts glutamate from an anabolic central metabolism role to an acid stress response role and was likely expressed as a protective mechanism to counter the high concentration of secreted organic acids (67). Similar responses have been observed during phosphate-limited growth, which also produces large amounts of organic acids (68).

Iron acquisition-related protein abundance. Iron-limited growth increased abundance of a number of iron acquisition-related proteins. Two isoforms of the membrane portion of the enterobactin transporter, FepA, were identified. Abundance of the FepA isoform eID 1274 demonstrated a strong increase under iron-limited conditions. The protein levels increased 10-fold from a D of 0.4 to 0.1 h^{-1} and were up to 17-fold greater ($P < 1.1 \times 10^{-16}$) than under glucose-limited growth at the same dilution rate. Alternatively, the abundance of the FepA isoform eID 1207 increased with decreasing dilution rate under both nutrient-limited conditions ($P < 0.02$); protein levels increased 4-fold more under glucose limitation and 1.5-fold under iron-limiting conditions between a D of 0.4 and 0.1 h^{-1}. At a D of 0.1 h^{-1}, the abundance of FhuA (a subunit of the ferrichrome transporter) was 2.1-fold higher for the iron-limited cultures than the glucose-limited cultures at the same dilution rate. FhuA abundance increased 2.5-fold under iron-limited growth from a D of 0.3 h^{-1} to 0.1 h^{-1} ($P < 1.1 \times 10^{-16}$). The outer membrane receptor for ferric 2,3-dihydroxybenzoylserine (CirA), an iron-siderophore complex uptake receptor (69), was found as two isoforms (eID 0051 and 0057). Both isoforms had higher protein levels under iron-limiting conditions (4- to 13-fold higher; $P < 1.1 \times 10^{-16}$) than the corresponding glucose-limited conditions (changes were larger for eID 0051). Changes in protein level as a function of dilution rate were no greater than 2-fold for either isoform under iron-limited conditions.

Two isoforms of the Fur-regulated iron storage protein bacterioferritin (Bfr) were found, one in the cytoplasmic fraction and one in the membrane fraction. The abundance of Bfr in the cytoplasmic fraction (eID 0405) was consistently higher during glu-

TABLE 2 Protein abundance as a function of nutrient limitation and chemostat dilution rate for discussed membrane spots

	Log10 normalized spot volumes[a]								Trends[b]							
	Glucose				Iron				Limitation across D[c]		Carbon vs. Iron, for each D					
ID_Gene name	0.1h^{-1}	0.2h^{-1}	0.3h^{-1}	0.4h^{-1}	0.1h^{-1}	0.2h^{-1}	0.3h^{-1}	0.4h^{-1}	Glc	Fe	0.10	0.20	0.30	0.40	Description
ID:0261_GapA	5.74± 0.35	5.48± 0.13	5.84± 0.15	5.72± 0.1	6.16± 0.24	5.87± 0.23	6.30± 0.09	6.25± 0.05							Glyceraldehyde 3-phosphate dehydrogenase-A
eID:0666_Pgk	5.65± 0.34	5.47± 0.22	5.67± 0.3	5.35± 0.18	6.00± 0.07	6.17± 0.21	6.13± 0.06	5.95± 0.08							Phosphoglycerate kinase
eID:1247_Eno	5.87± 0.23	5.69± 0.09	6.04± 0.26	5.78± 0.1	6.35± 0.1	6.44± 0.12	6.37± 0.07	6.09± 0.11							Enolase
ID:0145_Eno	5.94± 0.26	5.76± 0.06	5.81± 0.2	5.57± 0.12	6.06± 0.12	6.20± 0.08	6.09± 0.05	5.86± 0.09							Enolase
eID:0852_SucD	5.65± 0.18	5.64± 0.27	5.58± 0.3	5.81± 0.21	4.99± 0.09	5.03± 0.2	4.94± 0.11	5.13± 0.13							Succinyl-CoA synthetase, α subunit
eID:0742_GadAB	5.38± 0.14	5.50± 0.1	5.54± 0.23	5.39± 0.12	5.50± 0.06	5.99± 0.2	5.94± 0.1	5.73± 0.06							Glutamate decarboxylase B
eID:1274_FepA	6.39± 0.21	6.44± 0.16	6.47± 0.25	6.40± 0.11	7.62± 0.17	7.27± 0.25	6.89± 0.22	6.62± 0.14							Ferric enterobactin OMP
eID:1207_FepA	6.13± 0.25	5.86± 0.08	5.67± 0.17	5.55± 0.07	5.70± 0.14	5.72± 0.2	5.66± 0.09	5.52± 0.11							Ferric enterobactin OMP
eID:0057_CirA	5.31± 0.29	5.45± 0.15	5.40± 0.07	5.55± 0.09	6.07± 0.18	6.00± 0.37	5.88± 0.18	6.10± 0.18							Ferric dihyroxybenzoylserine transport Outer membrane receptor
eID:0051_CirA	5.18± 0.29	5.48± 0.13	5.45± 0.17	5.69± 0.15	6.36± 0.21	6.28± 0.37	6.10± 0.2	6.34± 0.19							Ferric dihyroxybenzoylserine transport Outer membrane receptor
eID:1257_TufA	6.52± 0.15	6.46± 0.15	6.36± 0.1	6.14± 0.07	6.49± 0.1	6.62± 0.21	6.47± 0.09	6.28± 0.07							Elongation Factor TU
eID:0961_TufA	5.78± 0.15	5.71± 0.12	5.39± 0.17	5.42± 0.11	5.47± 0.13	5.63± 0.12	5.31± 0.19	5.45± 0.2							Elongation Factor TU
eID:1053_FusA	5.28± 0.3	5.09± 0.24	5.01± 0.18	4.83± 0.24	5.90± 0.12	5.77± 0.14	5.36± 0.19	5.19± 0.26							Elongation Factor G
ID:0117_GroL	5.76± 0.24	5.75± 0.08	5.58± 0.15	5.52± 0.19	5.21± 0.22	5.20± 0.09	5.09± 0.15	5.06± 0.21							GroEL, chaperone Hsp60, peptide-dependent ATPase, heat shock protein
eID:1184_GroL	5.73± 0.32	5.79± 0.12	5.60± 0.13	5.45± 0.15	5.54± 0.21	5.69± 0.14	5.58± 0.12	5.43± 0.17							GroEL, chaperone Hsp60, peptide-dependent ATPase, heat shock protein
eID:0759_GroL	6.38± 0.18	6.64± 0.16	6.57± 0.1	6.44± 0.16	6.53± 0.23	6.81± 0.14	6.69± 0.09	6.55± 0.12							GroEL, chaperone Hsp60, peptide-dependent ATPase, heat shock protein
ID:0229_MalE	5.27± 0.45	4.95± 0.24	5.10± 0.25	5.2±0 .21	4.60± 0.16	4.61± 0.26	4.71± 0.19	4.70± 0.24							Maltose ABC transporter - periplasmic binding
eID:0996_MalE	5.41± 0.37	5.39± 0.22	5.15± 0.14	5.18± 0.18	4.80± 0.13	4.98± 0.16	4.78± 0.11	4.74± 0.19							Maltose ABC transporter - periplasmic binding
eID:0956_MglB	5.65± 0.67	5.16± 0.1	5.10± 0.22	5.06± 0.18	5.19± 0.24	4.98± 0.13	5.18± 0.07	5.16± 0.17							Galactose transport (ABC periplasmic)
eID:0959_MglB	5.28± 0.36	5.11± 0.1	4.89± 0.23	4.69± 0.14	5.19± 0.09	5.32± 0.1	5.19± 0.06	5.07± 0.19							Galactose transport (ABC periplasmic)
eID:0376_AceA	6.46± 0.31	6.40± 0.09	6.35± 0.3	6.2±0 .15	6.03± 0.12	6.08± 0.14	6.05± 0.12	5.88± 0.11							Isocitrate Lyase
ID:0152_AceA	6.12± 0.2	5.99± 0.1	5.84± 0.18	5.73± 0.09	5.85± 0.08	6.02± 0.07	5.90± 0.14	5.83± 0.13							Isocitrate Lyase
eID:1093_AceB	5.25± 0.34	5.15± 0.24	4.98± 0.27	4.92± 0.13	4.97± 0.21	5.18± 0.27	4.95± 0.2	5.00± 0.13							Malate synthase A
eID:0317_Acs	5.66± 0.21	5.50± 0.2	5.36± 0.11	5.33± 0.15	5.19± 0.14	5.20± 0.18	5.19± 0.13	5.25± 0.19							Acetyl-CoA synthetase
eID:0609_AcnB	5.6±0 .23	5.44± 0.17	5.33± 0.17	5.39± 0.16	5.82± 0.14	5.68± 0.2	5.43± 0.21	5.46± 0.17							Bifunctional aconitate hydratase 2/2-methylisocitrate dehydratase
ID:0402_Bfr	5.33± 0.23	5.1±0 .11	5.18± 0.25	4.82± 0.17	5.16± 0.15	5.41± 0.23	5.41± 0.11	5.01± 0.11							Bacterioferritin monomer
ID:0061_FhuA	5.82± 0.16	5.96± 0.15	5.92± 0.2	6.02± 0.14	6.14± 0.21	5.98± 0.25	5.75± 0.18	6.02± 0.16							Outer Membrane Protein Assembly Complex

[a] Means ± 3 SEM.

[b] Trends are plotted on the same scale for each spot and lines. Comparisons with a shaded background contain at least one statistically significant difference across the conditions ($P < 0.05$). The complete protein data set can be found in the supplemental material.

[c] From left to right, $D = 0.1$ to 0.4 h^{-1}.

TABLE 3 Protein abundance as a function of nutrient limitation and chemostat dilution rate for discussed cytoplasmic protein spots

	Log10 normalized spot volumes[a]								Trends[b]						
	Glucose				Iron				Limitation across D[c]		Carbon vs. Iron, for each D				
ID_Gene name[d]	0.1h^{-1}	0.2h^{-1}	0.3h^{-1}	0.4h^{-1}	0.1h^{-1}	0.2h^{-1}	0.3h^{-1}	0.4h^{-1}	Glc	Fe	0.10	0.20	0.30	0.40	Description
eID:0967_PykF	5.26± 0.09	5.21± 0.16	5.40± 0.2	5.36± 0.08	5.63± 0.16	5.46± 0.08	5.49± 0.14	5.48± 0.09							Pyruvate kinase I
ID:0200_PflB	5.54± 0.08	5.47± 0.16	5.72± 0.14	5.61± 0.14	5.60± 0.14	5.83± 0.09	5.91± 0.16	5.79± 0.15							Pyruvate formate-lyase
eID:0504_PflB	5.16± 0.14	5.17± 0.19	5.45± 0.16	5.20± 0.24	5.32± 0.22	5.53± 0.18	5.55± 0.24	5.27± 0.36							Pyruvate formate-lyase
eID:1343_GapA	5.85± 0.17	5.74± 0.21	5.72± 0.34	5.55± 0.44	6.17± 0.17	6.03± 0.29	5.78± 0.34	5.55± 0.48							Glyceraldehyde 3-phosphate dehydrogenase-A
eID:2245_GltA	5.11± 0.13	5.10± 0.15	5.26± 0.2	5.09± 0.26	4.65± 0.22	4.52± 0.21	4.79± 0.19	4.64± 0.2							Citrate synthase monomer
eID:0568_SucD	5.40± 0.28	5.03± 0.27	5.27± 0.28	5.54± 0.21	4.81± 0.33	4.58± 0.31	4.88± 0.2	5.05± 0.16							Succinyl-CoA synthetase, α subunit
eID:0443_Wrba	5.73± 0.17	5.67± 0.12	5.41± 0.15	5.66± 0.13	5.47± 0.29	5.52± 0.19	5.34± 0.45	5.45± 0.51							NAD(P)H:quinone oxidoreductase
eID:1676_SodA	5.78± 0.18	5.76± 0.15	5.85± 0.17	5.96± 0.12	5.37± 0.15	5.69± 0.15	5.81± 0.11	5.82± 0.13							superoxide dismutase (Mn)
eID:0099_SodB	5.42± 0.15	5.65± 0.26	5.16± 0.36	4.92± 0.48	4.88± 0.18	5.26± 0.22	4.81± 0.13	4.73± 0.11							Superoxide dismutase (Fe)
eID:2195_Dps	5.59± 0.1	5.47± 0.05	5.17± 0.11	5.11± 0.13	4.89± 0.1	5.15± 0.19	5.10± 0.1	5.10± 0.15							DNA binding protein
ID:0571_Dps	4.67± 0.1	4.68± 0.14	4.43± 0.15	4.5±0 .17	4.32± 0.19	4.64± 0.13	4.58± 0.11	4.62± 0.18							DNA binding protein
eID:0915_GadAB	5.68± 0.25	5.75± 0.21	5.84± 0.2	5.83± 0.08	5.66± 0.13	6.08± 0.13	5.97± 0.16	5.96± 0.19							Glutamate decarboxylase
eID:0191_TufA	5.48± 0.37	5.57± 0.12	5.13± 0.43	5.35± 0.73	5.44± 0.54	5.92± 0.23	5.42± 0.25	5.56± 0.54							Elongation Factor TU
eID:1229_TufA	6.19± 0.19	6.08± 0.23	6.02± 0.2	5.91± 0.09	6.22± 0.17	6.03± 0.21	6.11± 0.19	5.95± 0.1							Elongation Factor TU
eID:0839_TufA‡	6.59± 0.12	6.83± 0.1	6.62± 0.12	6.60± 0.14	6.56± 0.31	6.71± 0.18	6.61± 0.11	6.60± 0.16							Elongation Factor TU
eID:0924_TufA‡	6.03± 0.2	5.95± 0.12	5.94± 0.14	5.82± 0.18	5.88± 0.12	5.96± 0.07	5.90± 0.11	5.79± 0.24							Elongation Factor TU
eID:0250_FusA	5.46± 0.14	5.70± 0.07	5.63± 0.26	5.80± 0.27	5.51± 0.11	5.49± 0.1	5.54± 0.26	5.74± 0.28							Elongation Factor G
eID:0605_AceB	6.37± 0.23	6.61± 0.26	6.12± 0.15	6.14± 0.15	6.09± 0.15	6.15± 0.16	5.90± 0.16	5.94± 0.22							Acetyl-CoA synthetase (AMP-forming)
eID:0573_Acs	5.25± 0.2	5.04± 0.26	5.28± 0.21	5.25± 0.19	4.72± 0.29	4.44± 0.26	5.08± 0.23	5.17± 0.12							Acetyl-CoA synthetase (AMP-forming)
eID:0572_Acs	5.29± 0.18	5.24± 0.15	5.33± 0.25	5.29± 0.27	4.87± 0.21	4.76± 0.18	5.12± 0.23	5.06± 0.15							Acetyl-CoA synthetase
eID:0405_Bfr	5.39± 0.13	5.49± 0.14	5.15± 0.17	5.17± 0.19	5±0.1 8	5.14± 0.12	4.89± 0.12	4.88± 0.26							Bacterioferritin monomer

[a] Means ± 3 SEM.
[b] Trends are plotted on the same scale for each spot. Plots with shaded backgrounds contain at least one statistically significant difference across the conditions ($P < 0.05$). The complete protein data set can be found in the supplemental material.
[c] From left to right, $D = 0.1$ to 0.4 h^{-1}.
[d] ‡ indicates protein spots that were <2-fold different across all conditions.

cose-limited growth than iron-limited growth and generally higher at lower dilution rates, with maximum abundance occurring at a D of 0.2 h^{-1}. The abundance of Bfr in the membrane fraction (ID 0402) was generally higher for iron-limited growth than glucose-limited growth. The abundance of membrane-associated Bfr declined 2.5-fold at 0.4 h^{-1} compared with 0.3 h^{-1} ($P < 1.1 \times 10^{-16}$). See Tables 2 and 3 for more information.

Outer membrane porin abundance during iron-limited growth. Four outer membrane porins (Omp) were identified (OmpF, OmpX, OmpC, and OmpA). Protein levels for the single identified outer membrane porin F spot (OmpF; eID 1249) were ~6 to 16-fold higher ($P < 1.1 \times 10^{-16}$) under glucose-limited conditions than during iron-limited growth for all dilution rates. Two outer membrane protein X (OmpX) isoforms (eID 1258 and 0310) were observed. Both isoforms were expressed at levels ~2- to 4-fold higher ($P < 0.01$) under iron-limited conditions than glucose-limited conditions. However, the single identified outer membrane porin C spot (OmpC; eID 0157) had protein levels that were 2- to 4-fold higher ($P < 1.1 \times 10^{-16}$) under glucose-limited growth than during iron-limited growth for all dilution rates.

The outer membrane protein A (OmpA) data highlight the richness of protein isoforms, the power of differential 2-dimensional proteomics, and the challenges of interpreting proteomics data. A total of 18 gel spots contained isoforms of OmpA. Of the 13 single-protein-containing spots, 12 OmpA isoforms were from the membrane fractions and one was from the cytoplasm. The protein abundance patterns were complicated, with some isoforms being unaffected by nutrient limitation or dilution rate (eID 1255, 1256, 0853, 0653, 0676, 0442, 0468, 0316, and 0645) and others showing changes. For instance, isoform eID 1111 was expressed at 2- to 5-fold-higher levels ($P < 0.03$) under glucose-limited conditions at all dilution rates compared to iron-limited growth. Considering the complexity of the data, general conclusions were difficult to make. While complex, the Omp data provide a view into the nuanced expression of different cellular strategies for interacting with the environment. The observations also contribute to the growing body of data examining transporter expression as a function of nutrient limitation (70–72). See the supplemental material for porin data.

Elongation factor and chaperone abundance during iron-limited growth. A number of regulator proteins (TufA, FusA, and GroL) were identified. All of these proteins had multiple isoforms complicating the interpretation of their role in stress adaptation. For example, the ribosomal elongation factor Tu (TufA) was found in 12 different protein spots. Of the six single-protein spots, four were in the cytoplasm fraction (eID 0924, 1229, 0839, and 0191) and two in the membrane fraction (eID 1257 and 0961). In addition, 6 other isoforms were found in multiprotein spots, suggesting a complicated biology for the protein. Generally, the single-protein spots showed an increase in protein levels with decreases in dilution rate. See Tables 2 and 3 for more information.

Patterns of abundance during glucose-limited growth. The abundance of alternative carbon source transporters was elevated during glucose-limited growth compared with iron-limited growth. An alternative sugar transporter, MalE (ID 0229; eID 0996), was expressed at 2- to 8-fold-higher levels ($P < 1.1 \times 10^{-16}$) during glucose-limited growth than iron-limited growth. The abundance of the ABC sugar transporter MglB (eID 0956 and 0959) also increased with decreasing growth rate for glucose-limited growth and was up 5- to 8-fold ($P < 0.02$) at a D of 0.1 h^{-1} compared with 0.4 h^{-1}. In addition, the previously mentioned OmpF and OmpC proteins levels increased significantly during glucose-limited growth.

There were indications that during glucose-limited growth, the glyoxylate shunt pathway was functioning. Abundance of isocitrate lyase, AceA (eID 0376), was 2- to 3-fold ($P < 0.01$) higher under glucose limitation for all dilution rates, while another isoform of AceA (ID 0152) was 2-fold higher ($P < 1.1 \times 10^{-16}$) only under glucose limitation at a D of 0.1 h^{-1}. Malate synthase, AceB (eID 0605), located in the cytoplasmic fraction was upregulated 1.5- to 3-fold ($P < 0.04$) for glucose-limited growth, but a membrane isoform (eID 1093) was expressed at higher levels during glucose limitation only at a D of 0.1 h^{-1} (2.3-fold; $P = 0.05$). Use of the glyoxylate shunt during carbon starvation was proposed previously to be part of the "hungry bacteria" adaptation and is consistent with *in silico* cellular economy analysis of central metabolism (39, 45, 73).

Acetyl coenzyme A (acetyl-CoA) synthetase (Acs) protein was found in the membrane (eID 0317) and the cytoplasmic fractions (eID 0572 and 0573). Levels of the membrane isoform increased with increasing glucose limitation stress and were 2.3-fold higher at a D of 0.1 h^{-1} than at 0.4 h^{-1} ($P < 1.1 \times 10^{-16}$). They were also 1.3- to 3-fold higher ($P < 0.02$) than during iron-limited growth at a D of 0.1 to 0.3 h^{-1}. The cytoplasmic isoforms of Acs did not exhibit dilution rate-responsive changes under glucose-limited conditions; however, both isoforms increased slightly with increasing dilution rate under iron limitation, reaching 1.4- to 2.3-fold increases at a D of 0.4 h^{-1} ($P < 0.04$) compared with 0.1 h^{-1}. Additionally, the abundance of these isoforms was generally 3- to 4-fold higher ($P < 1.1 \times 10^{-16}$) under glucose-limited than under iron-limited conditions at dilution rates of 0.1 to 0.2 h^{-1}. For glucose-limited conditions, these observations could relate to a strategy to prevent loss of acetate from the central metabolism or a strategy to utilize any exogenous acetate (74). See Tables 2 and 3 for more information.

DISCUSSION

E. coli acclimation to iron-limited growth and glucose-limited growth was studied at four distinct levels of stress using chemostat cultivation. Iron is a trace element that is used as an enzymatic cofactor and is distributed unevenly across central metabolism enzymes; glucose, under the conditions investigated, is both a carbon source and the sole energy source and is required to synthesize every enzyme (Fig. 5). Iron-limited growth and carbon-limited growth represent an interesting contrast in microbial nutrient limitation responses. The stress gradients produced physiological responses that changed as a function of both limitation type and stress severity. A cellular economic analysis of the inherent tradeoffs between metabolic pathway synthesis requirements (nutrient investment into pathway proteins) and the energetic efficiencies of the pathway (ATP per substrate catabolized) provides a theoretical framework for interpreting the results and explaining why certain metabolic strategies have been selected by evolution. This theme has been explored previously using an *in silico* analysis of different nutrient investment strategies as a function of culturing conditions (45, 46, 75).

When iron is abundant and glucose is scarce, it is competitive from an economic and ecological perspective to make the most efficient use of the limiting resource. Efficient use of glucose to make biomass translates into a high biomass-per-glucose yield

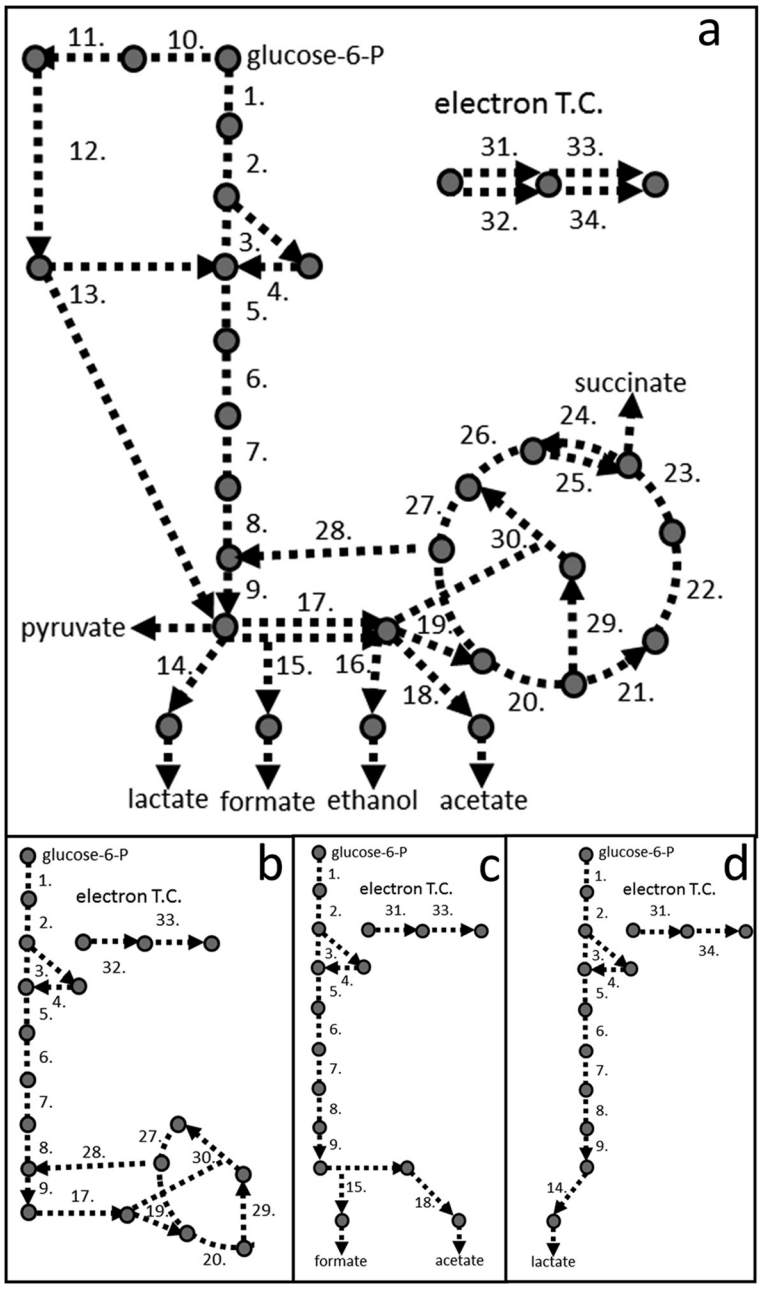

Rxn.	Protein	A. acids	Iron	ATP,ē
1.	2 Pgi	1098	0	0,0
2.	4 PfkA	1280	0	-,0
3.	2 FbaA	718	0	0,0
4.	2 TpiA	510	0	0,0
5.	4 GapA	1324	0	0,+
6.	1 Pgk	387	0	+,0
7.	2 GpmA	500	0	0,0
8.	2 Eno	864	0	0,0
9.	4 PykF	1880	0	+,0
10.	1 Zwf	491	0	0,+
11.	1 Pgl	331	0	0,0
12.	1 Edd	603	0	0,0
13.	3 Eda	639	0	0,0
14.	1 LdhA	329	0	0,-
15.	2 PflB	1520	0	0,0
16.	2 AdhE	1782	2	0,-
17.	24 AceE, 24 AceF, 12 LpdA	42096	0	0,+
18.	2 Pta, 1 AckA	1828	0	+,0
19.	6 GltA	2562	0	0,0
20.	2 AcnB	1730	4	0,0
21.	2 IcdA	832	0	0,+
22.	12 SucA, 24 SucB, 2 LpdA	21864	0	0,+
23.	2 SucC, 2 SucD	1332	0	+,0
24.	1 SdhA, 1 SdhB, 1 SdhC, 1 SdhD	1068	10	0,+
25.	1FrdA, 1FrdB, 1 FrdC, 1 FrdD	1096	9	0,-
26.	2 FumA	1868	0	0,0
27.	2 MdH	624	0	0,+
28.	1 PcK	540	0	-,0
29.	4 AceA	1774	0	0,0
30.	1 AceB	533	0	0,0
31.	1 Ndh	434	0	0,-
32.	1 NuoA, 1 NuoB, 1 NuoC, 1 NuoD, 1 NuoE, 1 NuoF, 1 NuoG, 1 NuoJ, 1 NuoK, 1 NuoL, 1 NuoM, 1 NuoN	4878	32	0,-
33.	1 CydA, 1 CydB	901	3	0,-
34.	1 CyoA, 1 CyoB, 1 CyoC, 1 CyoD	1291	2	0,-

FIG 5 (a) Diagram of *E. coli* central metabolism. Circles represent metabolites, and numbers correspond to the enzyme-catalyzed reactions listed at right. Enzyme data include enzyme or subunit name, subunit composition for a functional enzyme (i.e., monomer, dimer, etc.), total amino acid (A. acids) count for the entire functional enzyme (used as a proxy for overall resource investment), total iron investment for entire functional enzyme, and whether the enzyme produces (+) or consumes (−) ATP or reducing equivalents (ē). The diagram does not include cofactors or biosynthetic pathways. (b) Proposed central metabolism for carbon-limited cells highlighting the use of the glyoxylate shunt instead of the full TCA cycle. Glucose-limited growth at a D of 0.1 h^{-1} likely included flux through reaction 15 (PflB). (c) Proposed central metabolism for iron-limited cells experiencing moderate nutrient scarcity stress. (d) Proposed central metabolism for iron-limited cells experiencing severe iron scarcity stress. T.C., transport chain.

(consistent with data in Fig. 3a) and efficient use of glucose to make energy translate into complete oxidation to carbon dioxide, with low yields of alternative metabolic by-products (consistent with data in Fig. 4). Cellular acclimation to glucose limitation also involved a shift from the full TCA cycle to the oxidative use of the glyoxylate shunt (Table 2). This transition is predicted using cellular economic theory, because the glyoxylate shunt (AceA and AceB) requires a smaller investment of resources (carbon and nitrogen) (Fig. 5b) to build, relative to the full TCA cycle, yet is very efficient at oxidizing glucose-derived metabolites.

Similar economic arguments can be made to interpret the iron-limited growth. The *E. coli* central metabolism is highly redundant, possessing numerous parallel pathways (45, 46), and these various pathways require different iron investments and have different catabolic efficiencies. Iron scarcity should penalize the use of nonessential pathways which require iron-containing

enzymes. While the Embden-Meyerhoff-Parnas (EMP) and Entner-Doudoroff (ED) glycolysis pathways do not require iron investment, many enzymes associated with respiratory metabolism do. Large iron investments are required to synthesize the enzymatic infrastructure of the TCA cycle (e.g., SdhB, FrdB, and FumB), portions of the intermediary metabolism (e.g., AdhE and FdhH), and proton pumping components of the electron transport chain (e.g., CyoB, CydA, and NuoG) (Fig. 5a) (41).

During iron-limited growth, the cellular metabolism was thought to shift from the high-ATP-yielding, iron-containing pathways to lower-ATP-yielding, simpler pathways that accomplish essential functions but do not require iron. Flux through the TCA cycle was presumably reduced, based on protein abundance patterns (Table 2) and published data (41). The electron transport chain, which did carry a significant flux based on electron balance calculations (see Table S2 in the supplemental material), was probably limited to the low-iron-requiring components, like the soluble Ndh, which does not pump any protons, as opposed to the iron-requiring membrane-associated Nuo complex. This low-iron-investment strategy would produce a smaller proton motive force per oxygen molecule consumed, translating into a lower P/O number (ratio of ATP formed to oxygen reduced) than high iron-investment strategies. While only minimal electron transport chain proteomics data were found in the current study, transcriptomic data for iron-limited growth have been reported for batch growth and demonstrated transitions in electron transport components which are consistent with the concept of investment tradeoffs as a function of iron scarcity (41). Under these conditions, it is more competitive, on an iron investment basis, to extract energy from glucose using glycolysis-based substrate-level phosphorylation and to secrete the partially oxidized by-products, which would otherwise require a large iron investment to further oxidize. The decrease in cellular ATP per glucose yields associated with a shift from a respiration-based to a substrate-level-based ATP phosphorylation strategy would require a concomitant increase in glucose catabolic rates to maintain the same ATP availability. These trends were observed under the iron-limited conditions, where increased iron scarcity led to increased specific glucose catabolic rates and increased lactate secretion (Fig. 3b and 4). The observed overflow metabolism represents a highly efficient use of the limiting resource iron.

Proteins associated with genes regulated by Fur and RhyB were observed in this work (a summary can be found in Table S5 in the supplemental material). A number of the protein abundance trends were consistent with previous transcript work (42, 76). For example, many TCA cycle enzyme abundances were down relative to those in glucose-limited growth, consistent with previous transcript results, and iron storage protein bacterioferrin (Bfr eID 0405) abundance decreased, consistent with its reported Fur regulation. However, a substantial increase in aconitate hydratase B (AcnB) abundance was observed under iron-limited conditions relative to glucose-limited conditions (Table 2). This observation was contrary to the transcript data from Massé et al. (42, 76), who reported that AcnB mRNA was regulated by the small RNA RhyB (42), suggesting that the abundance of AcnB should go down under iron-limiting conditions. *E. coli* has two aconitate hydratase enzymes to catalyze the essential TCA cycle conversion of citrate to isocitrate (77, 78). AcnA possesses enhanced stability to oxidants, and it is expressed under oxidative stress conditions and repressed under iron-limiting conditions (78, 79), leaving only AcnB to function under iron-limited conditions. Low iron levels would reduce the occurrence of the Fenton reaction and therefore hydroxyl radical generation, perhaps decreasing the need for AcnA. Additionally, the observed increase in AcnB abundance corresponds to a suggested role of AcnB as an iron sensor (79). The ferrichrome transporter (FhuA) is believed to be regulated by Fur, but not strongly, and has been a source of some confusion (14, 41). The current work, through the use of a gradient of iron stress, found that FhuA abundance changes were complex, suggesting that the previous observations may have varied due to different levels of culture iron scarcity.

Lactate secretion has been observed in the opportunistic human pathogen *Staphylococcus aureus* under iron-limited conditions (80). The Gram-positive organism *S. aureus* is a competent mixed-acid fermenter and possesses the enzymatic machinery to secrete an array of by-products. The *S. aureus* study proposed that lactate (lactic acid) was secreted to lower the local pH, facilitating the release of iron bound by host proteins. The present research and ongoing metabolic modeling offer an alternative explanation to the acidification theory (75). Under conditions of iron limitation, these two generalist microbes (*E. coli* and *S. aureus*) shift their pathways to enzymes that require less of the limiting nutrient iron. The adoption of a fermentation-like overflow metabolism which secretes lactate is a competitive investment of scarce iron, based on the genome-encoded potential of these Gram-negative and Gram-positive microorganisms.

Microbial metabolic responses to iron scarcity are critical in a wide range of ecosystems from medical infections to marine nutrient cycling. This critical nutrient represents a powerful yet poorly characterized experimental system for general studies of competitive microbial acclimations to nutrient-limiting environments and for specific studies of pathogen strategies for growth and persistence in mammalian host tissue with low iron bioavailability.

ACKNOWLEDGMENTS

We thank Reed Taffs for his technical assistance, helpful discussions, and manuscript editing; Jonathan Hilmer, Walid Maaty, and the Mass Spectrometry, Proteomics & Metabolomics Facility in the Montana State University Department of Chemistry and Biochemistry for technical support and services, Matthew Shipman for proteomics protocol assistance, Mark Burr for providing the ammonium assay protocol, Luis Serrano and Abigail Richards for assistance with the CAS assay, and Edward Dratz, Brian Bothner, Ashley Beck, and Kristopher Hunt for careful manuscript reading and helpful discussions. We also thank Zdye LLC for the generous gift of Zdyes used in this work.

This work was funded by the NIH CoBRE (P20RR024237) and the NSF IGERT (DGE 0654336) programs. The Murdock Charitable Trust has provided generous support for the instrumentation in the Mass Spectrometry Facility.

We have no conflicting financial interests to declare.

REFERENCES

1. **Ames BN.** 2006. Low micronutrient intake may accelerate the degenerative diseases of aging, allocation of scarce micronutrients by triage. Proc. Natl. Acad. Sci. U. S. A. **103:**17589–17594. http://dx.doi.org/10.1073/pnas.0608757103.
2. **Elser JJ, Bracken MES, Cleland EE, Gruner DS, Harpole WS, Hillebrand H, Ngai JT, Seabloom EW, Shurin JB, Smith JE.** 2007. Global analysis of nitrogen and phosphorus limitation of primary producers in freshwater, marine and terrestrial ecosystems. Ecol. Lett. **10:**1135–1142. http://dx.doi.org/10.1111/j.1461-0248.2007.01113.x.
3. **Kazemi Seresht A, Palmqvist EA, Olsson L.** 2011. The impact of phos-

phate scarcity on pharmaceutical protein production in *S. cerevisiae*: linking transcriptomic insights to phenotypic responses. Microb. Cell Fact. **10:**104. http://dx.doi.org/10.1186/1475-2859-10-104.
4. **Elser JJ, Acquisti C, Kumar S.** 2011. Stoichiogenomics: the evolutionary ecology of macromolecular elemental composition. Trends Ecol. Evol. **26:**38–44. http://dx.doi.org/10.1016/j.tree.2010.10.006.
5. **Sterner RW, Elser JJ.** 2002. Ecological stoichiometry: the biology of elements from molecules to the biosphere. Princeton University Press, Princeton, NJ.
6. **Makino W, Cotner JB, Sterner RW, Elser JJ.** 2003. Are bacteria more like plants or animals? Growth rate and resource dependence of bacterial C:N:P stoichiometry. Funct. Ecol. **17:**121–130. http://dx.doi.org/10.1046/j.1365-2435.2003.00712.x.
7. **Zinn M, Witholt B, Egli T.** 2004. Dual nutrient limited growth: models, experimental observations, and applications. J. Biotechnol. **113:**263–279. http://dx.doi.org/10.1016/j.jbiotec.2004.03.030.
8. **Baudouin-Cornu P, Surdin-Kerjan Y, Marlière P, Thomas D.** 2001. Molecular evolution of protein atomic composition. Science **293:**297–300. http://dx.doi.org/10.1126/science.1061052.
9. **Bragg JG, Wagner A.** 2009. Protein material costs: single atoms can make an evolutionary difference. Trends Genet. **25:**5–8. http://dx.doi.org/10.1016/j.tig.2008.10.007.
10. **Archibald F.** 1983. *Lactobacillus plantarum*, an organism not requiring iron. FEMS Microbiol. Lett. **19:**29–32. http://dx.doi.org/10.1111/j.1574-6968.1983.tb00504.x.
11. **Posey JE, Gheridini FC.** 2000. Lack of a role for iron in the Lyme disease pathogen. Science **288:**1651–1653. http://dx.doi.org/10.1126/science.288.5471.1651.
12. **Chipperfield JR, Ratledge C.** 2000. Salicylic acid is not a bacterial siderophore: a theoretical study. BioMetals **13:**165–168. http://dx.doi.org/10.1023/A:1009227206890.
13. **Boukhalfa H, Crumbliss AL.** 2002. Chemical aspects of siderophore mediated iron transport. BioMetals **15:**325–339. http://dx.doi.org/10.1023/A:1020218608266.
14. **Hantke K.** 1981. Regulation of ferric iron transport in Escherichia coli K12: isolation of a constitutive mutant. Mol. Gen. Genet. **182:**288–292. http://dx.doi.org/10.1007/BF00269672.
15. **Weinberg ED.** 1975. Nutritional immunity—host's attempt to withhold iron from microbial invaders. JAMA **231:**39–41. http://dx.doi.org/10.1001/jama.1975.03240130021018.
16. **Kehl-Fie TE, Skaar EP.** 2010. Nutritional immunity beyond iron: a role for manganese and zinc. Curr. Opin. Chem. Biol. **14:**218–224. http://dx.doi.org/10.1016/j.cbpa.2009.11.008.
17. **Schaible UE, Kaufmann SHE.** 2004. Iron and microbial infection. Nat. Rev. Microbiol. **2:**946–953. http://dx.doi.org/10.1038/nrmicro1046.
18. **Skaar EP.** 2010. The battle for iron between bacterial pathogens and their vertebrate hosts. PLoS Pathog. **6:**e1000949. http://dx.doi.org/10.1371/journal.ppat.1000949.
19. **Litwin CM, Calderwood SB.** 1993. Role of iron in regulation of virulence genes. Clin. Microbiol. Rev. **6:**137–149.
20. **Abdul-Tehrani Hudson AJ, Yung-Sheng C, Timms AR, Hawkins C, Williams JM, Harrison PM, Guest JR, Andrews SC.** 1999. Ferritin mutants of *Escherichia coli* are iron deficient and growth impaired, and *fur* mutants are iron deficient. J. Bacteriol. **181:**1415–1428.
21. **Michel KP, Pistorius EK.** 2004. Adaptation of the photosynthetic electron transport chain in cyanobacteria to iron deficiency: the function of IdiA and IsiA. Physiol. Plant. **120:**36–50. http://dx.doi.org/10.1111/j.0031-9317.2004.0229.x.
22. **Bullen J, Griffiths E, Rogers H, Ward G.** 2000. Sepsis: the critical role of iron. Microbes Infect. **2:**409–415. http://dx.doi.org/10.1016/S1286-4579(00)00326-9.
23. **Andrews SC, Robinson AK, Rodríguez-Quiñones F.** 2003. Bacterial iron homeostasis. FEMS Microbiol. Rev. **27:**215–237. http://dx.doi.org/10.1016/S0168-6445(03)00055-X.
24. **Newton SMC, Igo JD, Scott DC, Klebba PE.** 1999. Effect of loop deletions on the binding and transport of ferric enterobactin by FepA. Mol. Microbiol. **32:**1153–1165. http://dx.doi.org/10.1046/j.1365-2958.1999.01424.x.
25. **Braun V, Braun M.** 2002. Iron transport and signaling in *Escherichia coli*. FEBS Lett. **529:**78–85. http://dx.doi.org/10.1016/S0014-5793(02)03185-X.
26. **Raymond KN, Dertz EA, Kim SS.** 2003. Enterobactin: an archetype for microbial iron transport. Proc. Natl. Acad. Sci. U. S. A. **100:**3584–3588. http://dx.doi.org/10.1073/pnas.0630018100.
27. **Smith AW.** 1998. Iron starvation and siderophore-mediated iron transport. Methods Microbiol. **27:**331–342. http://dx.doi.org/10.1016/S0580-9517(08)70294-0.
28. **Erdner DL, Anderson DM.** 1999. Ferredoxin and flavodoxin as biochemical indicators of iron limitation during open-ocean iron enrichment. Limnol. Oceanogr. **44:**1609–1615. http://dx.doi.org/10.4319/lo.1999.44.7.1609.
29. **Herbert D, Elsworth R, Telling RC.** 1956. The continuous culture of bacteria; a theoretical and experimental study. J. Gen. Microbiol. **14:**601–622. http://dx.doi.org/10.1099/00221287-14-3-601.
30. **Novick A, Szilard L.** 1950. Description of the chemostat. Science **112:**715–716. http://dx.doi.org/10.1126/science.112.2920.715.
31. **Boer VM, Crutchfield CA, Bradley PH, Botstein D, Rabinowitz JD.** 2010. Growth-limiting intracellular metabolites in yeast growing under diverse nutrient limitations. Mol. Biol. Cell **21:**198–211. http://dx.doi.org/10.1091/mbc.E09-07-0597.
32. **O'Farrell PH.** 1975. High resolution two-dimensional electrophoresis of proteins. J. Biol. Chem. **250:**4007–4021.
33. **Shevchenko A, Jensen ON, Podtelejnikov AV, Sagliocco F, Wilm M, Vorm O, Mortensen P, Boucherie H, Mann M.** 1996. Linking genome and proteome by mass spectrometry: Large-scale identification of yeast proteins from two dimensional gels. Proc. Natl. Acad. Sci. U. S. A. **93:**14440–14445. http://dx.doi.org/10.1073/pnas.93.25.14440.
34. **Dürrschmid K, Reischer H, Schmidt-Heck W, Hrebicek T, Guthke R, Rizzi A, Bayer K.** 2008. Monitoring of transcriptome and proteome profiles to investigate the cellular response of *E. coli* towards recombinant protein expression under defined chemostat conditions. J. Biotechnol. **135:**34–44. http://dx.doi.org/10.1016/j.jbiotec.2008.02.013.
35. **Lok C-N, Ho C-M, Chen R, He Q-Y, Yu W-Y, Sun H, Tam PK-H, Chiu J-F, Che C-M.** 2006. Proteomic analysis of the mode of antibacterial action of silver nanoparticles. J. Proteome Res. **5:**916–924. http://dx.doi.org/10.1021/pr0504079.
36. **Lüders S, Fallet C, Franco-Lara E.** 2009. Proteome analysis of the *Escherichia coli* heat shock response under steady-state conditions. Proteome Sci. **7:**36. http://dx.doi.org/10.1186/1477-5956-7-36.
37. **Schliep M, Ryall B, Ferenci T.** 2012. The identification of global patterns and unique signatures of proteins across 14 environments using outer membrane proteomics of bacteria. Mol. Biosyst. **8:**3017–3027. http://dx.doi.org/10.1039/c2mb25212k.
38. **Tang Y, Quail MA, Artymiuk PJ, Green J.** 2002. *Escherichia coli* aconitases and oxidative stress: post-transcriptional regulation of *sodA* expression. Microbiology **148:**1027–1037. http://mic.sgmjournals.org/content/148/4/1027.long.
39. **Wick LM, Quadroni M, Egli T.** 2001. Short- and long-term changes in proteome composition and kinetic properties in a culture of *Escherichia coli* during transition from glucose-excess to glucose limited growth conditions in continuous culture and vice versa. Environ. Microbiol. **3:**588–599. http://dx.doi.org/10.1046/j.1462-2920.2001.00231.x.
40. **Golec P, Karczewska-Golec J, Voigt B, Albrecht D, Schweder T, Hecker M, Węgrzyn G, Łoś M.** 2013. Proteomic profiles and kinetics of development of bacteriophage T4 and its *rI* and *rIII* mutants in slowly growing *Escherichia coli*. J. Gen. Virol. **94:**896–905. http://dx.doi.org/10.1099/vir.0.048686-0.
41. **McHugh JP, Rodríguez-Quiñones F, Hossein A-T, Svistunenko DA, Poole RK, Cooper CE, Andrews SC.** 2003. Global iron-dependent gene regulation in *Escherichia coli*: a new mechanism for iron homeostasis. J. Biol. Chem. **278:**29478–29486. http://dx.doi.org/10.1074/jbc.M303381200.
42. **Massé E, Gottesman S.** 2002. A small RNA regulates the expression of genes involved in iron metabolism in *Escherichia coli*. Proc. Natl. Acad. Sci. U. S. A. **99:**4620–4625. http://dx.doi.org/10.1073/pnas.032066599.
43. **Ihssen J, Egli T.** 2004. Specific growth rate and not cell density controls the general stress response in *Escherichia coli*. Microbiology **150:**1637–1648. http://dx.doi.org/10.1099/mic.0.26849-0.
44. **Ihssen J, Egli T.** 2005. Global physiological analysis of carbon- and energy-limited growing *Escherichia coli* confirms a high degree of catabolic flexibility and preparedness for mixed substrate utilization. Environ. Microbiol. **7:**1568–1581. http://dx.doi.org/10.1111/j.1462-2920.2005.00846.x.
45. **Carlson RP.** 2007. Metabolic systems cost-benefit analysis for interpreting network structure and regulation. Bioinformatics **23:**1258–1264. http://dx.doi.org/10.1093/bioinformatics/btm082.
46. **Carlson RP.** 2009. Decomposition of complex microbial behaviors into

resource-based stress responses. Bioinformatics **25:**90–97. http://dx.doi.org/10.1093/bioinformatics/btn589.
47. **Flamholz A, Noor E, Bar-Even A, Liebermeister W, Milo R.** 2013. Glycolytic strategy as a tradeoff between energy yield and protein cost. Proc. Natl. Acad. Sci. U. S. A. **110:**10039–10044. http://dx.doi.org/10.1073/pnas.1215283110.
48. **Molenaar D, van Berlo R, de Ridder D, Teusink B.** 2009. Shifts in growth strategies reflect tradeoffs in cellular economics. Mol. Syst. Biol. **5:**323. http://dx.doi.org/10.1038/msb.2009.82.
49. **Holzhutter HG.** 2004. The principle of flux minimization and its application to estimate stationary fluxes in metabolic networks. Eur. J. Biochem. **271:**2905–2922. http://dx.doi.org/10.1111/j.1432-1033.2004.04213.x.
50. **Ausubel F, Brent R, Kingston R, Moore D, Seidman JG, Smith JA, Struhl K (ed).** 1992. Short protocols in molecular biology, 2nd ed. Greene Publishing Associates and John Wiley & Sons, New York, NY.
51. **Riemer J, Hoepken HH, Czerwinska H, Robinson SR, Dringen R.** 2004. Colorimetric ferrozine-based assay for the quantitation of iron in cultured cells. Anal. Biochem. **331:**370–375. http://dx.doi.org/10.1016/j.ab.2004.03.049.
52. **Liu X, Ferenci T.** 1998. Regulation of porin-mediated outer membrane permeability by nutrient limitation in *Escherichia coli*. J. Bacteriol. **180:**3917–3922.
53. **Senn H, Lendenmann U, Snozzi M, Hamer G, Egli T.** 1994. The growth of *Escherichia coli* in glucose-limited chemostat cultures: a re-examination of the kinetics. Biochim. Biophys. Acta **1201:**424–436. http://dx.doi.org/10.1016/0304-4165(94)90072-8.
54. **Searle PL.** 1984. The Berthelot or indophenol reaction and its use in the analytical chemistry of nitrogen: a review. Analyst **109:**549–568. http://dx.doi.org/10.1039/an9840900549.
55. **Stieg S.** 2005. 4500-NH_3 F phenate method, p 4–114. *In* Eaton AD, Clesceri LS, Rice EW, Greenberg AE, Franson MAH (ed), Standard methods for the examination of water and wastewater, 21st (centennial) ed. American Public Health Association/American Water Works Association/Water Environment Federation, Washington, DC.
56. **Schwyn B, Neilands JB.** 1987. Universal chemical assay for the detection and determination of siderophores. Anal. Biochem. **160:**47–56. http://dx.doi.org/10.1016/0003-2697(87)90612-9.
57. **Dratz EA, Grieco PA.** January 2004. Zwitterionic dyes for labeling in proteomic and other biological analyses. US patent 7,582,260.
58. **Shipman M, Lubick K, Fouchard D, Guram R, Grieco P, Jutila M, Dratz EA.** 2012. Proteomic and systems biology analysis of monocytes exposed to securinine, a $GABA_A$ receptor antagonist and immune adjuvant. PLoS One **7:**e41278. http://dx.doi.org/10.1371/journal.pone.0041278.
59. **Candiano G, Bruschi M, Musante L, Santucci L, Ghiggeri GM, Carnemolla B, Orecchia P, Zardi L, Righetti PG.** 2004. Blue silver: a very sensitive colloidal Coomassie G-250 staining for proteome analysis. Electrophoresis **25:**1327–1333. http://dx.doi.org/10.1002/elps.200305844.
60. **Hartmann A, Braun V.** 1981. Iron uptake and iron limited growth of *Escherichia coli* K-12. Arch. Microbiol. **130:**353–356. http://dx.doi.org/10.1007/BF00414599.
61. **Alexander ML, Ramkrishna D.** 1991. Cybernetic modeling of iron limited growth and siderophore production. Biotechnol. Bioeng. **38:**637–652. http://dx.doi.org/10.1002/bit.260380609.
62. **Castan A, Sven-Olof E.** 2002. Formate accumulation due to DNA release in aerobic cultivations of *Escherichia coli*. Biotechnol. Bioeng. **77:**324–328. http://dx.doi.org/10.1002/bit.1198.
63. **De Maeseneire SL, De Mey M, Vandedrinck S, Vandamme EJ.** 2006. Metabolic characterization of *E. coli* citrate synthase and phosphoenolpyruvate carboxylase mutants in aerobic cultures. Biotechnol. Lett. **28:**1945–1953. http://dx.doi.org/10.1007/s10529-006-9182-8.
64. **Alexeeva S, de Kort B, Sawers G, Hellingwerf KJ, Teixeira JM.** 2000. Effects of limited aeration and of the ArcAB system on intermediary pyruvate catabolism in *Escherichia coli*. J. Bacteriol. **182:**4934–4940. http://dx.doi.org/10.1128/JB.182.17.4934-4940.2000.
65. **Alexeeva S, Hellingwerf KJ, de Mattos MJT.** 2002. Quantitative assessment of oxygen availability: perceived aerobiosis and its effect on flux distribution in the respiratory chain of *Escherichia coli*. J. Bacteriol. **184:**1402–1406. http://dx.doi.org/10.1128/JB.184.5.1402-1406.2002.
66. **Sauer U, Lasko DR, Fiaux J, Hochuli M, Glaser R, Szyperski T, Wüthrich K, Bailey JE.** 1999. Metabolic flux ratio analysis of genetic and environmental modulations of *Escherichia coli* central carbon metabolism. J. Bacteriol. **181:**6679–6688.
67. **Lin J, Smith MP, Chapin KC, Baik HS, Bennett GN, Foster JW.** 1996. Mechanisms of acid resistance in enterohemorrhagic Escherichia coli. Appl. Environ. Microbiol. **62:**3094–3100.
68. **Moreau PL.** 2007. The lysine decarboxylase CadA protects *Escherichia coli* starved of phosphate against fermentation acids. J. Bacteriol. **189:**2249–2261. http://dx.doi.org/10.1128/JB.01306-06.
69. **Griggs DW, Tharp BB, Konisky J.** 1987. Cloning and promoter identification of the iron-regulated *cir* gene of *Escherichia coli*. J. Bacteriol. **169:**5343–5352.
70. **Alteri CJ, Mobley HLT.** 2007. Quantitative profile of the uropathogenic *Escherichia coli* outer membrane proteome during growth in human urine. Infect. Immun. **75:**2679–2688. http://dx.doi.org/10.1128/IAI.00076-06.
71. **Hagan EC, Mobley HLT.** 2007. Uropathogenic *Escherichia coli* outer membrane antigens expressed during urinary tract infection. Infect. Immun. **75:**3941–3949. http://dx.doi.org/10.1128/IAI.00337-07.
72. **Molloy MP, Herbert BR, Slade MB, Rabilloud T, Nouwens AS, Williams KL, Gooley AA.** 2000. Proteomic analysis of the *Escherichia coli* outer membrane. Eur. J. Biochem. **267:**2871–2881. http://dx.doi.org/10.1046/j.1432-1327.2000.01296.x.
73. **Fischer E, Sauer U.** 2003. A novel metabolic cycle catalyzes glucose oxidation and anaplerosis in hungry *Escherichia coli*. J. Biol. Chem. **278:**46446–46451. http://dx.doi.org/10.1074/jbc.M307968200.
74. **Hua Q, Yang C, Oshima T, Mori H, Shimizu K.** 2004. Analysis of gene expression in *Escherichia coli* in response to changes of growth-limiting nutrient in chemostat cultures. Appl. Environ. Microbiol. **70:**2354–2366. http://dx.doi.org/10.1128/AEM.70.4.2354-2366.2004.
75. **Carlson RP, Taffs RL.** 2010. Molecular-level tradeoffs and metabolic adaptation to simultaneous stressors. Curr. Opin. Biotechnol. **21:**670–676. http://dx.doi.org/10.1016/j.copbio.2010.05.011.
76. **Massé E, Vanderpool CK, Gottesman S.** 2005. Effect of RyhB small RNA on global iron use in *Escherichia coli*. J. Bacteriol. **187:**6962–6971. http://dx.doi.org/10.1128/JB.187.20.6962-6971.2005.
77. **Blank L, Green J, Guest JR.** 2002. AcnC of *Escherichia coli* is a 2-methylcitrate dehydratase (PrpD) that can use citrate and isocitrate as substrates. Microbiology **148:**133–146. http://mic.sgmjournals.org/content/148/1/133.long.
78. **Gruer MJ, Guest JR.** 1994. Two genetically-distinct and differentially-regulated aconitases (AcnA and AcnB) in *Escherichia coli*. Microbiology **140:**2531–2541. http://dx.doi.org/10.1099/00221287-140-10-2531.
79. **Varghese S, Tang Y, Imlay JA.** 2003. Contrasting sensitivities of *Escherichia coli* aconitases A and B to oxidation and iron depletion. J. Bacteriol. **185:**221–230. http://dx.doi.org/10.1128/JB.185.1.221-230.2003.
80. **Friedman DB, Stauff DL, Pishchany G, Whitwell CW, Torres VJ, Skaar EP.** 2006. *Staphylococcus aureus* redirects central metabolism to increase iron availability. PLoS Pathog. **2:**e87. http://dx.doi.org/10.1371/journal.ppat.0020087.